

Mechanical Structuring of Lithium-Ion Battery Electrodes Using an Embossing Roller

Josef Keilhofer,* Leon Wolfgang Ferdinand Schaffranka, Amy Wuttke, Florian Josef Günter, Lucas Hille, Filip Adam Dorau, and Rüdiger Daub

Highly performing lithium-ion batteries are essential for the electrification of the transport sector. However, the two performance criteria, high power density and high energy density, inversely correlate with each other via the mass loading of the electrodes. To achieve high charging and discharging rates at high energy densities, structuring of electrodes is a proven method. Currently, structures are mostly realized by laser ablation, which comes along with material loss and low process rates. Herein, a concept for electrode structuring through mechanical embossing in a high-throughput roll-to-roll process is elaborated. Different integration options are described and the challenges are discussed. To provide a proof of concept, a hand-operated embossing device is built and used to structure graphite anodes. In a rate capability test, an increase in discharge capacity at medium C-rates by up to 14.3% is observed.

1. Introduction

Lithium-ion batteries are a key technology for replacing fossil fuels in energy storage applications.^[1] To penetrate markets besides consumer electronics, the application-specific requirements for the battery cell as a product must be met. For electromobility, energy density and rate capability are crucial performance criteria.^[2] However, optimizing both properties independently is challenging and intrinsically limited.^[3] High-loaded electrodes ensure a high energy density and hence a long driving range, while the rate capability is low for those kinds of electrodes.^[4] Structuring is a promising approach to increase the rate capability of high-loaded electrodes without influencing the energy density. With this electrode treatment, the diffusion

limitation of lithium-ions in the electrolyte liquid is tackled and hence the intrinsic limit for rate capability is shifted.^[5] Thus, higher power densities can be achieved without sacrificing the energy density. Alternatively, by increasing the electrode loading and compensating for the accompanying losses in power density by structuring, the energy density can also be increased. Furthermore, postmortem measurements indicated less lithium plating of structured electrodes.^[6–8] Lithium plating can lead to an internal short circuit and thermal runaway of the cell. With operational safety as a strict criterion in battery cell quality, structured electrodes show a high potential for implementation in the industry. This advantageous electrode

treatment was already patented in 2012, giving different proposals for creating the structures. These include crack formation by targeted drying, additive manufacturing by 3D printing, laser ablation, and mechanical structuring with an embossing roller.^[9] Part of these proposals have been examined in the literature such as 3D printing^[10] and laser structuring.^[11–17] Additionally, further alternative methods for creating structured electrodes, such as micromilling,^[18] screen printing,^[19] or pore forming via a foaming agent,^[20] were described. However, the structuring methods investigated so far either cannot directly control the structure geometry or suffer from low throughput. Laser ablation is the most widely used method for creating structured electrodes in the literature. The reason for its low throughput is that the laser beam must be directed individually to each hole position via a scanner. Approaches such as parallelization of multiple laser systems or polygon scanners significantly increase the throughput, but could not achieve the web speeds necessary for industrial mass production so far.^[21] For the mass production of lithium-ion battery cells, the challenge is to find scalable and robust solutions rather than high flexibility in process design.^[22]

To do so for high-power density cells, in this work, a method for mechanically structuring lithium-ion battery electrodes in a roll-to-roll process is investigated. A concept for the additional process is elaborated and different integration options are discussed. A proof of concept is provided by structuring lithium-ion battery electrodes with a hand-operated embossing device. These structured electrodes are investigated in a rate capability test.

J. Keilhofer, L. W. F. Schaffranka, A. Wuttke, F. J. Günter, L. Hille, F. A. Dorau, R. Daub
Institute for Machine Tools and Industrial Management (iwb)
Technical University of Munich
Boltzmannstrasse 15, 85748 Garching, Germany
E-mail: Josef.Keilhofer@iwb.tum.de

 The ORCID identification number(s) for the author(s) of this article can be found under <https://doi.org/10.1002/ente.202200869>.

© 2023 The Authors. Energy Technology published by Wiley-VCH GmbH. This is an open access article under the terms of the Creative Commons Attribution-NonCommercial-NoDerivs License, which permits use and distribution in any medium, provided the original work is properly cited, the use is non-commercial and no modifications or adaptations are made.

DOI: 10.1002/ente.202200869

2. Concept Section

2.1. Description of the Process Concept

The concept comprises two rollers arranged vertically above each other. The upper roller is provided with a negative structure and hence can introduce structures into the coating of an electrode passed between the two rollers, as illustrated in **Figure 1**. The mating roller may, in the case of double-side coated electrodes, also exhibit a negative structure. Its vertical position is fixed while the position of the upper roller can be adjusted according to the requirements for the structuring process. The applied pressure of the upper roller in combination with an adjustable stop defines the maximum penetration depth of the negative structures into the electrode. The circulation speed of both rollers is precisely matched to the web speed of the electrode. As electrode defects can be mitigated by elevated temperatures,^[23,24] the rollers may also be heated. Additional elements such as deflection rollers, drawing rollers, and web edge guide control stabilize the process.

2.2. Integration into the Process Chain of Electrode Production

Figure 1 shows a schematic drawing of the investigated process in the case of single-side coated electrodes as well as possible integration options into the conventional process chain of electrode production. Comparable to laser structuring, there are several integration options.^[25] Integration is possible as a subprocess directly into an existing roll-to-roll process step of the electrode production such as coating or calendaring (options A to D). Alternatively, the additional process can also be operated in a standalone system (options B to D).

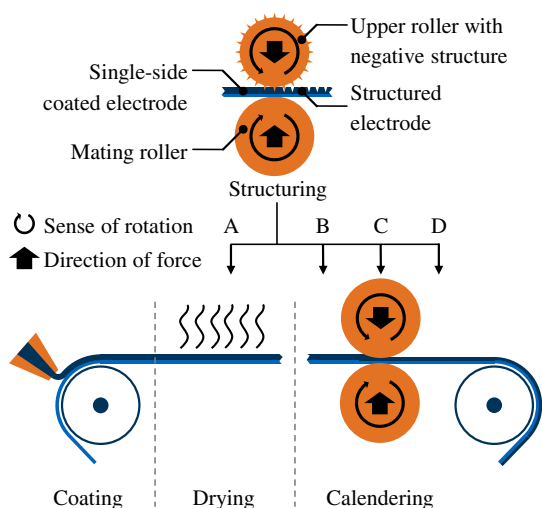


Figure 1. Schematic drawing of the concept for mechanically structuring single-side coated electrodes using an embossing roller. The conventional process chain of electrode production and four different integration options for the embossing process are depicted: A) During drying, B) after drying/before calendaring, C) during calendaring, and after D) calendaring. Depending on the option, structuring is integrated either as a standalone process step or inline as a subprocess in the conventional process chain.

Since electrode slurries may adhere to the embossing roller in a nondried state, mechanical insertion of the structures is only possible after sufficient predrying. Therefore, the structuring process can only be integrated from the drying process onward.

However, semidry conditions are assumed to be advantageous, as electrode deformation is easier in this state. Structuring should be carried out after the film shrinkage step, during which the particles of the electrode approach each other. After this drying step, the electrode structure does not change anymore as the active material particles are fixed by adjacent particles.^[26] Thus, the implementation as a subprocess could be realized by splitting up the drying line and inserting the embossing roller in between (see option A). However, this comes with a loss in flexibility, since the required degree of drying has to be reached within the first part of the drying line. Several coating properties such as solid content, wet film thickness, web speed, etc. influence the degree of drying and may have to be adjusted according to the position of the integrated roller.

Another option is to introduce the structures in the fully dried state (see option B). This allows greater flexibility for different production scenarios. In the case of inline integration, the structuring process can either be added after the drying section or before the calendaring process. However, structuring prior to calendaring may lead to clogging of the structures in the calendaring step.

This leads to the third option of integration after calendaring (c.f. option D), avoiding clogging of the structures. However, it is expected that high line loads are required to insert structures into already compacted electrodes, which can lead to higher wear and a more complex plant design.

Since with this option, the electrode surface is no longer adjustable in downstream process steps, problems can arise if the negative structures only partially penetrate. As a result, material can also be displaced toward the electrode's surface, creating edge protrusions around the introduced structures.

A fourth option is to combine structuring and calendaring in one process step (see option C). In this case, full penetration of the negative structures is necessary. Thus, the base surface from which the negative structures protrude must be perfectly flat, as this determines the final electrode surface. Irregularities at the surface of the anode can lead to local overpotentials, causing lithium plating.^[27] Furthermore, the flexibility of this process option is limited. If the electrode design is changed, it is mandatory to change the roller as well, since the depth of the negative structure must match the final thickness of the electrode. However, the combination of calendaring and structuring in one process is most advantageous from a cost perspective.

Generally, the alternative process can be readily integrated into the process chain, as it is very similar to the existing process of calendaring.

2.3. Roller Contamination and Wear

Although anode and cathode production lines are often operated separately in industrial battery cell factories and therefore cross-contamination is excluded, deposits on the negative structure must be strictly avoided. Residues on the embossing roller can lead to irregular structures and agglomerates on the electrode. Additionally, the penetration depth will be impacted by

residues on the embossing roller as the upper roller will be lifted if additional material enters the gap. This punctuated local stress on the roller might even lead to damage to the negative structure of the roller.

To avoid deposits, a special design of the surface of the structures may be chosen or a mechanism for inline cleaning of the roller must be implemented. Options to clean the roller are compressed air and brushes, both in combination with a suction system. Laser cleaning is an alternative as it is especially suited for small particles. Depending on the material properties, laser cleaning can selectively remove deposits without affecting the surface underneath.^[28]

Another challenge is roller wear, which is a well-known phenomenon in calendaring, especially in the case of cathodes due to the rigid particles. Having fine negative structures on its surface, wear is a particularly critical challenge of an embossing roller. To avoid downtime, it is important to track this gradual change of the negative structures. In addition, it must be known when to change the roller to avoid unacceptable losses in electrode quality.

Especially for embossing rollers, quality assurance is difficult as the relation between the monitoring surface size and the defect size is large. It is difficult to estimate the lifetime of an embossing roller without validation within a destructive long-time experiment.

2.4. Influence on the Throughput

The integration of the additional process step into an existing roll-to-roll process influences the throughput in different ways. First of all, an additional process leads to more effort in determining the process parameters and increases the ramp-up time. Maintenance may have to be carried out more frequently and is more time-consuming if an additional step is added to the process chain. Furthermore, the increased complexity due to additional interdependencies within the process chain increases the susceptibility to errors. All these factors may increase the downtime of the production line.

However, higher electrode loadings can be chosen, since the corresponding losses in rate capability are compensated by structuring. Thus, throughput in terms of produced energy storage capacity ($\text{MWh}_{\text{Cell}} \text{h}^{-1}$) is increased for most of the process steps, being one of the greatest levers for cost reduction.^[29] Additionally, reduced wetting times in the electrolyte filling step were reported for cells with structured electrodes.^[30–32] It can be assumed that mechanical structuring using embossing rollers can reach higher throughputs in comparison to other structuring techniques such as laser ablation.

3. Experimental Section

3.1. Electrode Preparation

For anode slurry preparation, distilled water was mixed with a thickener (Na-CMC; $M_w = 250\,000 \text{ g mol}^{-1}$; Merck) in a disperser (Dispermat FM 10; VMA-Getzmann) at 2000 rpm (tangential speed $v_{\text{tang}} = 6.8 \text{ m s}^{-1}$) until a homogeneous binder solution was obtained. Graphite (SMG-A5; Showa Denko) and conductive additive (C-Nergy Super C65; Imerys) were dry mixed

at 1400 rpm for 1 min in a rotary revolution mixer (Speedmixer DAC 1100.2 VAC-P; Hauschild) and added to the binder solution. After 45 min of mixing with 1500 rpm, a rubber binder (SBR BM-451-B; Zeon) was added and mixed with the blend for another 15 min at a speed of 250 rpm ($v_{\text{tang}} = 0.85 \text{ m s}^{-1}$). The solid content of the anode slurry was estimated to 52 wt%.

To prepare the cathode slurry, *N*-Methyl-2-pyrrolidone (NMP; anhydrous; 99.5%; Merck) was mixed with polyvinylidene fluoride (PVDF Solef 5130; Solvay) in the disperser at 2000 rpm ($v_{\text{tang}} = 6.8 \text{ m s}^{-1}$) until a homogeneous binder solution was obtained. NCM (HED NCM-622 DT011; BASF), conductive additive (C-Nergy Super C65; Imerys), and conductive graphite (C-Nergy SFG6L; Imerys) were mixed at 1400 rpm for 1 min in the rotary revolution mixer and added to the binder solution. The mixture was stirred for 60 min at 1500 rpm. The solid content of the cathode slurry was estimated to 78 wt%. The temperature during mixing in the disperser was kept below 25 °C by cooling for both slurries. After mixing, a degassing step was performed in the rotary revolution mixer for 5 min at 600 rpm and 250 mbar for both slurries.

The anode slurry and cathode slurry were coated onto a copper current collector foil (12 μm ; Cu-PHC; Schlenk) and aluminum current collector foil (15 μm ; Al-8079; Korff), respectively, using a tape casting lab coater (MSK-AFA-III; MTI). Drying was performed in a ventilated oven (Mehrzweck-Heissluftofen; Bartscher) at 50 °C for at least 30 min. The composition and the properties of the resulting electrodes are listed in Table 1.

3.2. Structuring and Calendaring

A hand-operated embossing device was built in-house at the *iwb* to structure electrodes (see Figure 2). The device consisted of two vertically arranged rollers (A) and (B). A manually operated spindle adjustment (C) allowed one to manipulate the load of the upper roller on the mating roller. It pressed a cover plate (D) onto two springs (E). The force was transferred to the bearings (F) of the upper roller pressing it onto the mating roller. The applied

Table 1. Composition and properties of single-side coated electrodes.

	anode		cathode		
	material	weight percent	material	weight percent	
composition	active material	graphite	94%	NMC622	95.5%
	binder	SBR	3%	PVDF	1.5%
	thickener/binder	CMC	2%	–	–
	conductive additive	C65	1%	C65	2.25%
	conductive graphite	–	–	SFG6L	0.75%
properties	porosity	30%		30%	
	mass loading (coating)	18.0 mg cm^{-2}		30.9 mg cm^{-2}	
	areal capacity	6.0 mA h cm^{-2}		5.0 mA h cm^{-2}	
	electrode diameter	15 mm		14 mm	
	current collector thickness	12 μm		15 μm	
	current collector material	copper		aluminum	

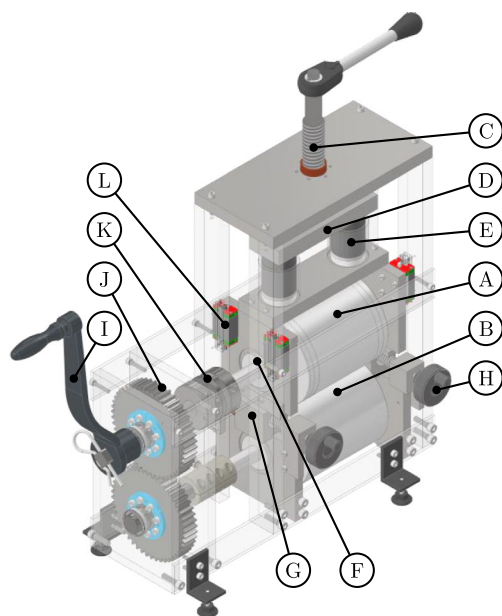


Figure 2. Illustration of the hand-operated embossing device used for manual electrode structuring. Key components are the upper roller possessing a negative structure (A), the mating roller (B), the spindle adjustment (C), the cover plate (D), the springs (E) for pressure regulation, the bearings (F), adjustable wedges (G), spindle adjustments (H) for gap control, a hand crank (I), a gear mechanism (J), a Schmidt offset coupling (K), and linear guides (L).

line load was determined via the compression of the springs and the spring constant.

To vary the roller gap, adjustable wedges (G) were located between the bearings of the upper and mating rollers. The position of the wedges can be manipulated by two hand-operated spindle adjustments (H), thus determining the distance between the upper and mating rollers. The rotary motion was generated by a hand crank (I) and transmitted to the mating roller via a gear mechanism (J). A Schmidt offset coupling (K) ensured constant angle-synchronous transmission at different levels of the upper roller. Linear guides (L) ensured that the position of the upper roller could only be varied in the vertical direction.

The upper roller exhibited a negative structure that is representatively shown in Figure 3. The topography data was recorded with a laser scanning microscope (VK 9710; Keyence). As the original roller did not fit into the measurement device due to geometrical limitations, a smaller roller, which was manufactured identically, was investigated. The pyramid-like (four-sided) structures were in a squared arrangement with a spacing of 220 μm . The height of the negative structures of the measured specimen was 100 μm .

To provide a proof of concept for integration option B as a stand-alone process (c.f. Figure 1), anodes were structured using the hand-operated embossing device with a line load of 64 N mm^{-1} . The gap was set to the corresponding thickness of the current collector (12 μm) to ensure that the full load was transferred to the electrode. The thickness of the anodes was reduced from (198 \pm 4) to (171 \pm 3) μm leading to a porosity of \approx 41%. No mass loss due to structuring was observed.

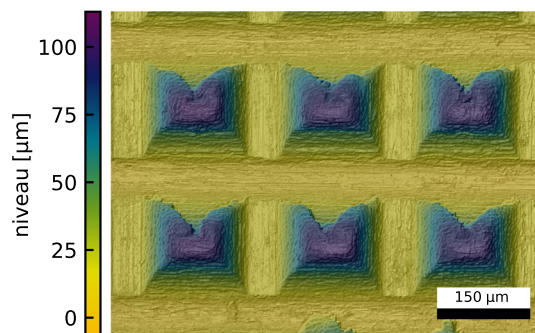


Figure 3. Topography of the negative structure of a roller processed identically to the upper roller of the embossing device. The structures are of pyramid-like shape (four-sided) in squared arrangement with a distance of 220 μm . Each structure element has a height of \approx 100 μm .

All electrodes were punched out (handheld punch; NOGAMI) and further compressed in a uniaxial hydraulic press (MP250D; Maassen) to a porosity of 30%.

3.3. Cell Assembly

Full cells (coin cells; 2032-type) were manufactured in an argon-filled glovebox (oxygen and water content <1 ppm; GS MEGA E-LINE; GS Glovebox). Anode (diameter 15 mm) and cathode (diameter 14 mm) were separated by two glass fiber separators (diameter 16 mm; Type 691; VWR). Additionally, two metal spacers with a total thickness of 1.5 mm were placed in the cell. 140 μL of electrolyte (LP572; 1 M LiPF_6 in EC:EMC 3:7 (wt:wt) +2% VC; BASF) was used per cell. Before assembling, all cell components were dried at 60 $^\circ\text{C}$ in the heatable exchange chamber of the glovebox. The electrodes and glass fiber separators were dried in a drying oven (B-585; Büchi) at 120 $^\circ\text{C}$. All drying steps were executed under vacuum at an absolute pressure of \approx 50 mbar.

3.4. Formation and Cell Testing

Cell testing was performed in a temperature-controlled chamber (ED-115; Binder) at 25 $^\circ\text{C}$ with a battery testing system (CTS; BaSyTec). After a wetting time of \approx 3 h, the formation was executed. Three charge and discharge cycles were performed at a constant current (CC) of 0.1 C between 2.9 and 4.2 V. The third charging cycle was followed by a constant voltage phase. One set of cells underwent a discharge rate capability test. Herein, the cells were charged at CC to the upper cutoff voltage of 4.2 V, followed by a constant voltage (CV) phase until the current dropped below 0.02 C. The cells were discharged at CC rates varying between 0.1 and 5 C until a minimum voltage of 2.9 V was reached. The testing procedure is described in detail in Table A1.

Another set of coin cells underwent a long-time cycling test after formation. For 12 times, a check-up cycle (both directions CCCV with 0.1 C) followed by 49 cycles (both directions CC with 0.5 C) was performed. The procedure is shown in detail in Table A2 in the appendix. All C-rates were calculated using the theoretical specific capacity of the cathode active material ($q_{\text{spec,NMC}} = 170 \text{ mA h g}^{-1}$).

4. Results

4.1. Electrode Morphology and Structure Analysis

The anodes were investigated using laser scanning microscopy after structuring and again after calendaring. In **Figure 4**, the obtained 2D images of the anode topography are shown. Additionally, cross sections through the topography of the respective electrodes are shown. The embossing roller process provides a regular pattern in a square arrangement with a spacing of 220 μm . The introduced structures exhibit a depth of 100 μm (58% of electrode coating thickness), indicating a full penetration of the negative structures. This is in accordance with the observed decrease in thickness due to structuring and shows that a replacement of the calendaring process (see integration option C in **Figure 1**) is possible if appropriate pressures are applied. After electrode compression, the structures are hardly recognizable as superficial clogging of the structures significantly reduced their width and depth.

4.2. Electrochemical Analysis

Additionally, the electrodes were investigated in a discharge rate capability test. In **Figure 5** the resulting discharge capacities over the cycle number are shown. At low C-rates (0.1–0.2 C), no significant differences in the discharge capacities were observed as Li-ion transport phenomena are not limiting at these C-rates. At medium C-rates, significant increases (+8.7% and +14.3% for 1 and 2 C, respectively) in the rate capability were achieved by anode structuring. The increase was calculated based on the last cycle of each C-rate as this cycle was affected the least by previous cycles at different C-rates. The results are in accordance with comparable works using laser ablation^[5,6,11,12,15] albeit the increase in discharge capacity is smaller due to the clogging of the structures. At high C-rates (here 3–5 C), structuring does

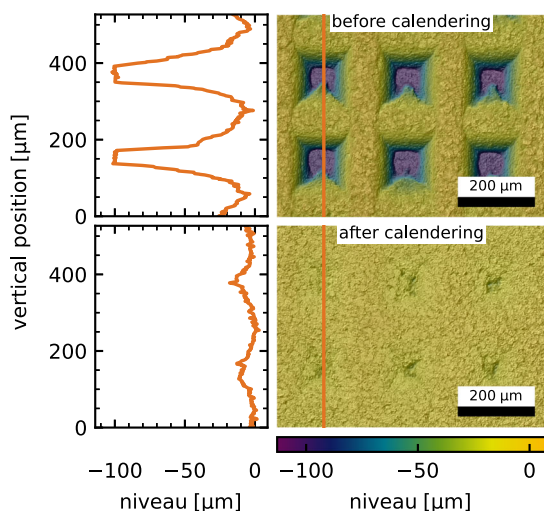


Figure 4. Topography data of the structured anode before calendaring (top) and after calendaring (bottom). On the right, the 2D image recorded with a laser scanning microscope is shown. The orange line marks the position of the cross section shown on the left.

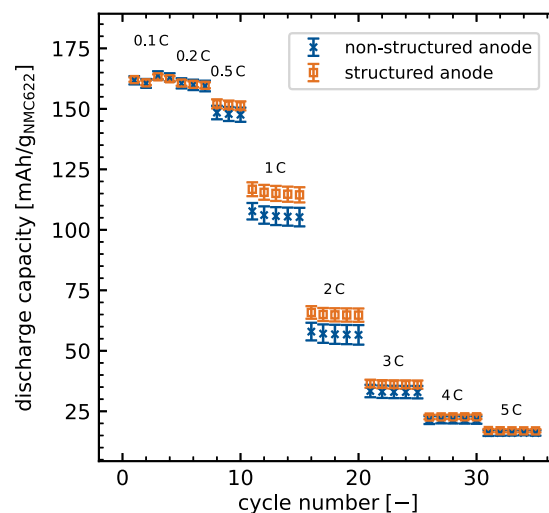


Figure 5. Discharge capacities during charging rate capability test for full cells with structured anodes compared to pristine anodes. The according C-rates are given in the graph. At the medium C-rate range, an increase in discharge capacity of the structured electrodes was observed. Error bars represent the standard deviation of five identical cells.

not affect the discharge capacity, which was also observed in simulations in literature.^[12] This effect is assigned to the high overpotential, which rapidly drives the cell into the cutoff voltage before significant lithium-ion transport via diffusion can occur. The origin of the high overpotential is due to lithium salt depletion in the electrolyte in the cathode close to the current collector which drastically slows down charge transfer kinetics. As a result, changing the transport properties in the electrode bulk material by structuring has hardly any influence at high C-rates.^[33]

The results of the long-time cycling test, comparing structured anodes to pristine anodes in full cells, are shown in **Figure 6**. Both anode types show a rapid decay in capacity. A reduced capacity retention can originate in loss of active material, loss of lithium inventory, or in increased internal cell resistances. The latter does not appear at lower C-rates where overpotentials are low, independent of the internal cell resistance. Hence, the capacity decay is caused by irreversible side reactions and lithium plating. The 80% state of health (SOH) limit is hit after 179 and 413 cycles for the reference cells and the cells with structured anodes respectively. The values were obtained by interpolating the mean capacity retention of the check-up cycles. Overall, the results show that structuring has no negative influence on long-time cycling. This is in accordance with literature that shows a positive impact on life-time due to structuring.^[8]

5. Conclusion

An alternative process concept for structuring lithium-ion battery electrodes using an embossing roller was presented. Possible integration options into the conventional process chain for the production of lithium-ion battery electrodes were

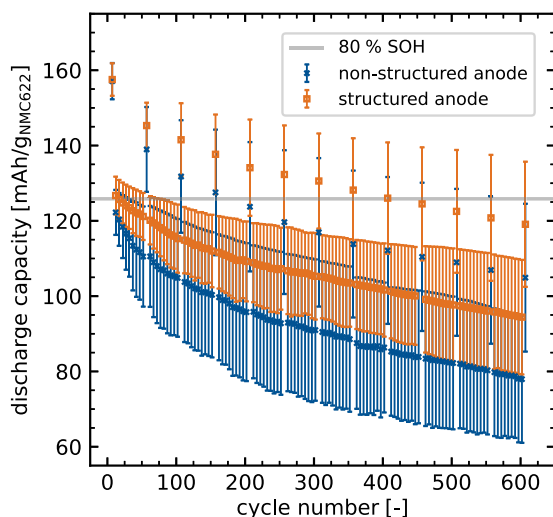


Figure 6. Discharge capacities during long-time cycling for full cells with structured anodes compared to pristine anodes. Charging and discharging were performed at a rate of 0.5 C. Every 50 cycles a 0.1 C check-up cycle was performed. The gray line marks the 80% SOH limit. Error bars represent the standard deviation of five identical cells.

discussed. The process represents a cost-effective alternative to laser structuring with high throughput as it can be used as a roll-to-roll process. Therefore, it has the potential to be used on an industrial scale for mass production. In most lithium-ion cell manufacturing process steps, structuring may enable higher throughput in $MWh_{Cell} h^{-1}$ because a higher electrode loading can be selected without sacrificing the power density. The associated losses in cell performance are compensated by structuring. The alternative process technology can allow for the mass production of batteries with both, high energy density and high power density. As these kinds of batteries are necessary for the automotive sector, the technology can contribute to the aim of replacing fossil fuels.

A proof of concept was provided by using a hand-operated embossing device to structure-dried electrodes. The structuring process simultaneously reduced the electrode thickness, indicating that both process steps, structuring and calendaring, can be combined if larger line loads compared to this study are applied. The introduced structures were clogged by the subsequent calendaring process. Nevertheless, an increase in discharge capacity at a C-rate of 2 C by 14.4% was achieved by structuring.

Further work is needed to enable the process for industrial application. In particular, the quality of the structured electrodes must be ensured in sustained continuous operation. Hence, questions concerning wear and deposits on the rollers must be clarified. Suitable measures may be roller cleaning, for example, with a laser. Optical analysis for example with push broom scanners can help to detect wear and deposits. In addition, a recurring analysis of the hole geometry in the electrodes would allow observing the roller degradation. If the challenges can be addressed, the industrial use of the alternative process can be economically advantageous.

Appendix A

Table A1. Cell testing procedure for discharge rate capability test including formation (CC = constant current, CV = constant voltage). Given voltages represent full cell voltage. C-rates are defined according to the theoretical capacity of the cathode.

repetitions	mode of operation	value	limit
2	charge (CC)	$I = 0.1 C$	$U = 4.2 V$
	discharge (CC)	$I = 0.1 C$	$U = 2.9 V$
2	charge (CC)	$I = 0.1 C$	$U = 4.2 V$
	charge (CV)	$U = 4.2 V$	$ I < 0.02 C$
	discharge (CC)	$I = 0.1 C$	$U = 2.9 V$
3	charge (CC)	$I = 0.2 C$	$U = 4.2 V$
	charge (CV)	$U = 4.2 V$	$ I < 0.02 C$
	discharge (CC)	$I = 0.2 C$	$U = 2.9 V$
3	charge (CC)	$I = 0.5 C$	$U = 4.2 V$
	charge (CV)	$U = 4.2 V$	$ I < 0.02 C$
	discharge (CC)	$I = 0.5 C$	$U = 2.9 V$
5	charge (CC)	$I = 0.5 C$	$U = 4.2 V$
	charge (CV)	$U = 4.2 V$	$ I < 0.02 C$
	discharge (CC)	$I = 1 C$	$U = 2.9 V$
5	charge (CC)	$I = 0.5 C$	$U = 4.2 V$
	charge (CV)	$U = 4.2 V$	$ I < 0.02 C$
	discharge (CC)	$I = 2 C$	$U = 2.9 V$
5	charge (CC)	$I = 0.5 C$	$U = 4.2 V$
	charge (CV)	$U = 4.2 V$	$ I < 0.02 C$
	discharge (CC)	$I = 3 C$	$U = 2.9 V$
5	charge (CC)	$I = 0.5 C$	$U = 4.2 V$
	charge (CV)	$U = 4.2 V$	$ I < 0.02 C$
	discharge (CC)	$I = 4 C$	$U = 2.9 V$
5	charge (CC)	$I = 0.5 C$	$U = 4.2 V$
	charge (CV)	$U = 4.2 V$	$ I < 0.02 C$
	discharge (CC)	$I = 5 C$	$U = 2.9 V$

Table A2. Cell testing procedure for long-time cycling test including formation (CC = constant current, CV = constant voltage). Given voltages represent full cell voltage. C-rates are defined according to the theoretical capacity of the cathode.

	repetitions	mode of operation	value	limit
formation	2	charge (CC)	$I = 0.1 C$	$U = 4.2 V$
		discharge (CC)	$I = 0.1 C$	$U = 2.9 V$
	1	charge (CC)	$I = 0.1 C$	$U = 4.2 V$
		charge (CV)	$U = 4.2 V$	$ I < 0.02 C$
		discharge (CC)	$I = 0.1 C$	$U = 2.9 V$

Table A2. Continued.

	repetitions	mode of operation	value	limit
cycling(12x)	1	charge (CC)	$I = 0.1 \text{ C}$	$U = 4.2 \text{ V}$
		charge (CV)	$U = 4.2 \text{ V}$	$ I < 0.02 \text{ C}$
		discharge(CC)	$I = 0.1 \text{ C}$	$U = 2.9 \text{ V}$
		discharge(CV)	$U = 2.9 \text{ V}$	$ I < 0.02 \text{ C}$
49	charge (CC)	$I = 0.5 \text{ C}$	$U = 4.2 \text{ V}$	
	discharge (CC)	$I = 0.5 \text{ C}$	$U = 2.9 \text{ V}$	

Acknowledgements

The authors gratefully acknowledge funding from the German Federal Ministry of Education and Research (BMBF) within the project ProfiStruk (grant number 03XP0244A). Thanks also goes to the internship participants Florian Bidlingmaier, Victor Cudmani, Kiyan Hadawi, Laurin Ködel, Simon Pfeiffer, and Ibrahim Shehadeh who assisted in the fabrication and preparation of the electrodes. Furthermore, the authors would like to thank the mechanical workshop of the *iwb*, in particular Armin Braun, Stefan Seidl, Andreas Grünwald, and Wolfgang Rissling, for manufacturing and optimizing the embossing device.

Open Access funding enabled and organized by Projekt DEAL.

Conflict of Interest

The authors declare no conflict of interest.

Data Availability Statement

The data that support the findings of this study are available from the corresponding author upon reasonable request.

Keywords

electrode designs, electrode structuring, lithium-ion batteries, microembossing

Received: August 1, 2022
Revised: February 27, 2023
Published online: March 23, 2023

- [1] *Future Trends in Production Engineering. German Academic Society for Production Engineering (WGP)* (Eds: G. Schuh, R. Neugebauer, E. Uhlmann), Springer, Berlin; Heidelberg [u.a.] **2013**, ISBN 978-3-642-24490-2, <https://publications.rwth-aachen.de/record/758932>.
- [2] D. Andre, S. J. Kim, P. Lamp, S. F. Lux, F. Maglia, O. Paschos, B. Stiaszny, *J. Mater. Chem. A* **2015**, *3*, 6709.
- [3] C. Heubner, M. Schneider, A. Michaelis, *Adv. Mater.* **2020**, *10*, 2.
- [4] A. Sakti, J. J. Michalek, E. R. Fuchs, J. F. Whitacre, *J. Power Sources* **2015**, *273*, 966.
- [5] L. Hille, H.-C. Toepfer, C. Schriever, J. Kriegler, J. Keilhofer, M. P. Noecker, M. F. Zaeh, *J. Electrochem. Soc.* **2022**, *169*, 060518.

- [6] J. B. Habedank, J. Kriegler, M. F. Zaeh, *J. Electrochem. Soc.* **2019**, *166*, A3940.
- [7] K. H. Chen, M. J. Namkoong, V. Goel, C. Yang, S. Kazemiabnavi, S. M. Mortuza, E. Kazyak, J. Mazumder, K. Thornton, J. Sakamoto, N. P. Dasgupta, *J. Power Sources* **2020**, *471*, 228475.
- [8] J. Kriegler, L. Hille, S. Stock, L. Kraft, J. Hagemeister, J. B. Habedank, A. Jossen, M. F. Zaeh, *Appl. Energy* **2021**, *303*, 117693.
- [9] U. Sauter, Battery e.g., Lithium Ion Battery has Porous Layered Electrode which is Provided with Several Recesses at Opposite Side of Electrode Metal Sheet **2014**, <https://register.dpma.de/DPMAregister/pat/PatSchrifteneinsicht?docId=DE102012215921A1> (accessed: February 2023).
- [10] C. Liu, F. Xu, X. Cheng, J. Tong, Y. Liu, Z. Chen, C. Lao, J. Ma, *Ceram. Int.* **2019**, *45*, 14188.
- [11] J. B. Habedank, J. Endres, P. Schmitz, M. F. Zaeh, H. P. Huber, *J. Laser Appl.* **2018**, *30*, 032205.
- [12] J. B. Habedank, L. Kraft, A. Rheinfeld, C. Krezdorn, A. Jossen, M. F. Zaeh, *J. Electrochem. Soc.* **2018**, *165*, A1563.
- [13] Y. Zheng, L. Pfäffl, H. J. Seifert, W. Pfleging, *Appl. Sci.* **2019**, *9*, 20.
- [14] J. Park, S. Hyeon, S. Jeong, H. J. Kim, *J. Ind. Eng. Chem.* **2019**, *70*, 178.
- [15] L. Hille, L. Xu, J. Keilhofer, S. Stock, J. Kriegler, M. F. Zaeh, *Electrochim. Acta* **2021**, *392*, 139002.
- [16] R. Dubey, M. D. Zwahlen, Y. Shynkarenko, S. Yakunin, A. Fuerst, M. V. Kovalenko, K. V. Kravchuk, *Batteries Supercaps* **2021**, *4*, 464.
- [17] M. Mangang, H. J. Seifert, W. Pfleging, *J. Power Sources* **2016**, *304*, 24.
- [18] E. R. Reale, K. C. Smith, *J. Electrochem. Soc.* **2018**, *165*, A1685.
- [19] A. Gören, J. Mendes, H. M. Rodrigues, R. E. Sousa, J. Oliveira, L. Hilliou, C. M. Costa, M. M. Silva, S. Lanceros-Méndez, *J. Power Sources* **2016**, *334*, 65.
- [20] R. Xiong, Y. Zhang, Y. Wang, L. Song, M. Li, H. Yang, Z. Huang, D. Li, H. Zhou, *Small Methods* **2021**, *5*, 2100280.
- [21] J. B. Habedank, D. Schwab, B. Kiesbauer, M. F. Zaeh, *J. Laser Appl.* **2020**, *32*, 022053.
- [22] A. Kwade, W. Haselrieder, R. Leithoff, A. Modlinger, F. Dietrich, K. Droeder, *Nat. Energy* **2018**, *3*, 290.
- [23] T. Günther, D. Schreiner, A. Metkar, C. Meyer, A. Kwade, G. Reinhart, *Energy Technol.* **2020**, *8*, 2.
- [24] A. Mayr, D. Schreiner, B. Stumper, R. Daub, *Procedia CIRP* **2022**, *107*, 295.
- [25] L. Hille, M. P. Noecker, B. Ko, J. Kriegler, J. Keilhofer, S. Stock, M. F. Zaeh, *J. Power Sources* **2023**, *556*, 232478.
- [26] S. Jaiser, A. Friske, M. Baunach, P. Scharfer, W. Schabel, *Drying Technol.* **2017**, *35*, 1266.
- [27] S. Müller, J. Eller, M. Ebner, C. Burns, J. Dahn, V. Wood, *J. Electrochem. Soc.* **2018**, *165*, A339.
- [28] A. C. Tam, W. P. Leung, W. Zapka, W. Ziemlich, *J. Appl. Phys.* **1992**, *71*, 3515.
- [29] F. Duffner, L. Mauler, M. Wentker, J. Leker, M. Winter, *Int. J. Prod. Econ.* **2021**, *232*, 107982.
- [30] W. Pfleging, J. Pröll, *J. Mater. Chem. A* **2014**, *2*, 14918.
- [31] J. Pröll, H. Kim, A. Piqué, H. J. Seifert, W. Pfleging, *J. Power Sources* **2014**, *255*, 116.
- [32] J. B. Habedank, F. J. Günter, N. Billot, R. Gilles, T. Neuwirth, G. Reinhart, M. F. Zaeh, *Int. J. Adv. Manufacturing Technology* **2019**, *102*, 2769.
- [33] M. J. Lain, E. Kendrick, *J. Power Sources* **2021**, *493*, 229690.